


Experimental verification of super-compact ultra-wideband (UWB) polarization and incident angle-independent metamaterial absorber

Manpreet Kaur and Hari Shankar Singh 

Department of Electronics and Communication Engineering, Thapar Institute of Engineering and Technology, Patiala 147 004, Punjab, India

Research Paper

Cite this article: Kaur M, Singh HS (2021). Experimental verification of super-compact ultra-wideband (UWB) polarization and incident angle-independent metamaterial absorber. *International Journal of Microwave and Wireless Technologies* **13**, 789–799. <https://doi.org/10.1017/S1759078720001300>

Received: 4 March 2020

Revised: 17 August 2020

Accepted: 18 August 2020

First published online: 15 September 2020

Key words:

Meta-materials; radar applications; ultra-wideband

Author for correspondence:

Hari Shankar Singh,

E-mail: harishankar1990@gmail.com

Abstract

In this paper, a super-compact ultra-wideband (UWB) metamaterial absorber (MMA) is presented. The absorber design consists of an inverted L-shaped structure and a diagonal rectangular-shaped structure. The capacitive coupling between these two structures not only provides UWB nature but also provides a super-compact absorber design. The dimension of the unit cell arrangement is $5 \times 5 \text{ mm}^2$ and printed on a low-cost FR-4 substrate of thickness 1.54 mm ($0.061\lambda_{\text{lowest}}$). The design absorber provides more than 97% absorptivity from 12 to 21 GHz for normal incidence electromagnetic (EM) wave. However, the proposed MMA has a full width at half maximum absorption bandwidth of 11.71 GHz from 10.34 to 22.05 GHz. Moreover, the surface current distributions have been analyzed to understand the absorption mechanism of the MMA. The stability of the proposed design is validated with different incident angles (for TE and TM modes) and different polarization angles. Finally, the absorber design is fabricated and verified experimentally. Furthermore, the UWB frequency range, high absorption, ease in design and fabrication, and cost-effective make it suitable for different quality applications in stealth technology, thermal imaging, radar detection, antenna systems, and other EM devices.

Introduction

Metamaterials are the artificial materials that exhibit the physical properties like negative permittivity and negative permeability [1] which are not present in ordinary materials. The metamaterial, being an unnatural structure has gained attentiveness in various applications such as perfect lens [2], cloaking [3], absorbers [4], and antenna size shrinking [5]. Further, the 2D planar structures of metamaterials i.e. metasurfaces are also used in various applications to enhance the antenna characteristics such as the gain of the antenna [6], the front-to-back ratio of the antenna [7], and many more. Over the last few years, a lot of work has been carried out over metamaterial absorber (MMA). However, small footprint, high peak absorption response, wide bandwidth, wide incident angle independent, and polarization-insensitive are still in the researcher's radar. Nevertheless, the wide bandwidth along with the small size is quite challenging for the researchers. However, numerous works have been carried out to get wide bandwidth but thicker substrate and large electrical footprint became a big constraint in many applications. In [8], a metamaterial decoupling cell has been incorporated in between the antenna array to enhance the isolation between the MIMO antenna elements. However, it may lead to the shifting of the resonance peak from its aimed frequency. Bhattacharyya *et al.* [9] and Wang *et al.* [10] have investigated absorber structures for a wideband response. However, the thickness of the substrate and non-flattop absorption limits their application. Moreover, lumped circuit elements [11, 12] have been incorporated at the top surfaces of the MMA to widen the bandwidth, however, this leads to fabrication complexity. In [13–15], a planar absorber structure has been presented to give a wider response. However, the limited bandwidth of the structure limits its application in various fields. In work [16], the absorber structure has been observed for presenting the wideband response. But the thickness of the structure is the biggest concern. Wang *et al.* [17] has investigated a meander wire structure loaded with resistors to provide a broader response. However, this meander wire structure and loaded resistors make the structure more complex. Further, the proposed absorber can also be compared with the structure having filter-like characteristics [18, 19]. It is known that the absorber and the filter both serve the same purpose of removing or eliminating the unwanted component from the signal. However, they are used in different applications. The absorber is used in applications like radar cross-section reduction, antenna, sensors, and many more whereas the filter is used in instrumentation, electronics, and communication systems especially in signal and image processing systems.

Table 1. Comparison table

References	Frequency range (GHz)	Size (mm ²)	Thickness	FWHM (GHz)
[9]	4.6–7.2	10 × 10	0.052 λ_{lowest} (λ_{lowest} at 4.9 GHz)	4
[10]	8.85–14.17	9 × 9	0.047 λ_{lowest} (λ_{lowest} at 8.85 GHz)	6.77
[11]	7.93–17.18	12 × 12	0.08 λ_{lowest} (λ_{lowest} at 8 GHz)	10.9
[12]	3.01–5.28	30 × 30	0.054 λ_{lowest} (λ_{lowest} at 3.27 GHz)	2.82
[13]	5.27–6.57	9 × 9	0.028 λ_{lowest} (λ_{lowest} at 5.34 GHz)	1.94
[14]	12.80–16.64	8 × 8	0.044 λ_{lowest} (λ_{lowest} at 13.2 GHz)	5.48
[15]	8.36–10.87	10 × 10	0.046 λ_{lowest} (λ_{lowest} at 8.75 GHz)	3.55
[16]	5.94–11.92	9 × 9	0.066 λ_{lowest} (λ_{lowest} at 6.2 GHz)	7.55
[17]	1.91–4.24	10 × 10	0.072 λ_{lowest} (λ_{lowest} at 2.16 GHz)	4.12
Proposed Design	12–21	5 × 5	0.061 λ_{lowest} (λ_{lowest} at 12 GHz) ^a	11.71

^aIt is slightly thicker as compared to other designs. However, it is compensated by the small size and ultrawide bandwidth.

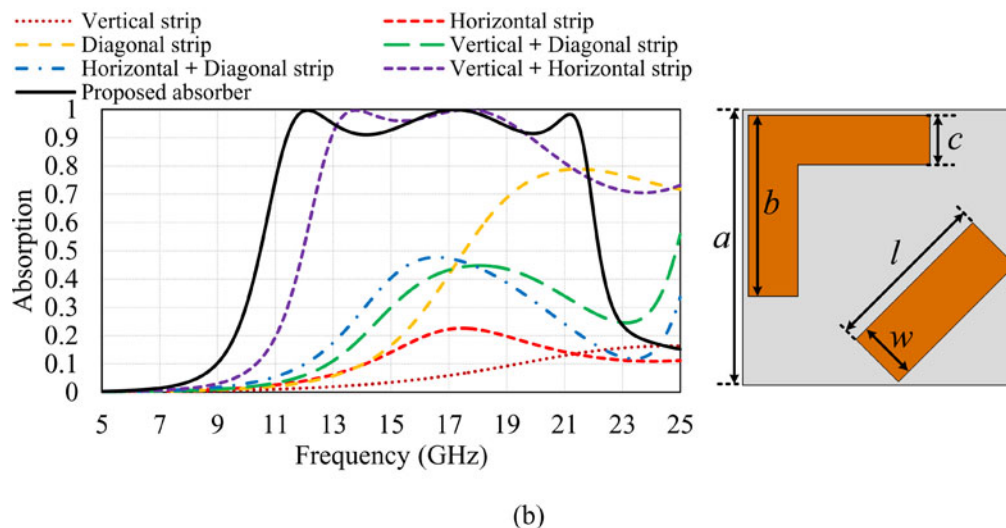
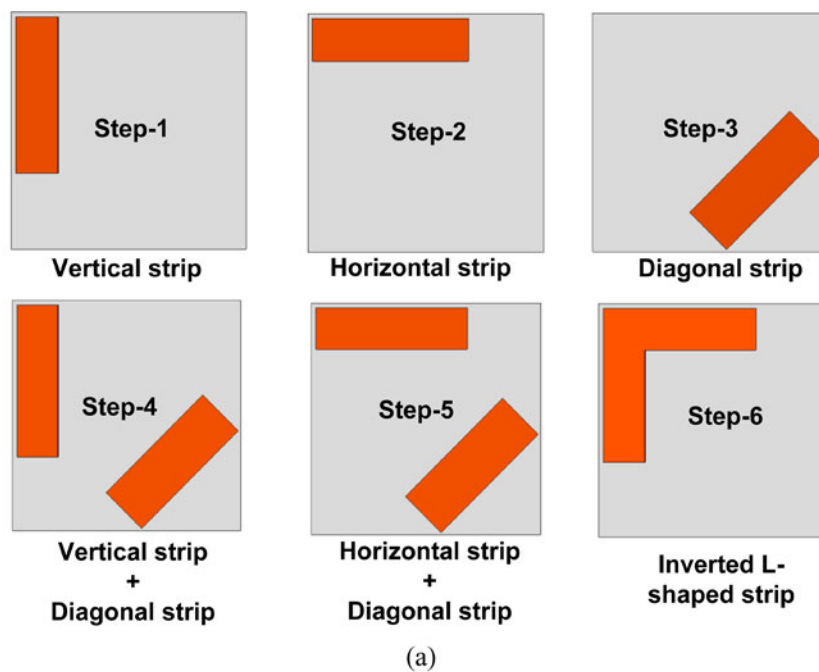


Fig. 1. (a) Design evolution of proposed absorber, (b) absorptivity corresponding to design steps. Detail dimensions are $a = 5$ mm, $b = 3.3$ mm, $c = 0.9$ mm, $l = 3$ mm, and $w = 1.1$ mm.

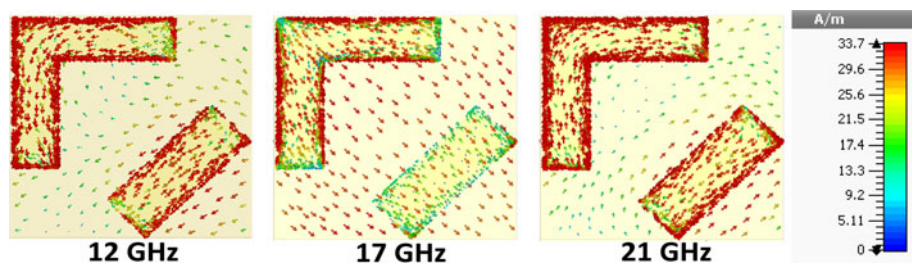


Fig. 2. Surface current distribution.

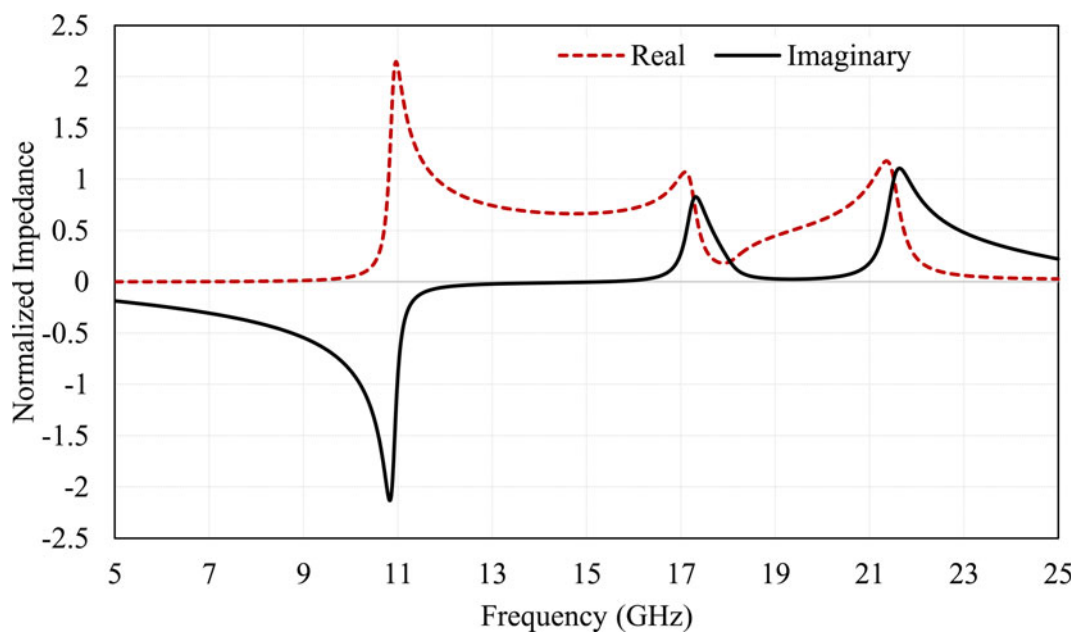


Fig. 3. Normalized input impedance of the proposed UWB absorber.

In this paper, a super-compact, polarization-insensitive ultra-wideband (UWB) MMA is designed. The proposed design comprises two resonating elements namely L-shaped strip and diagonal rectangular strip. The MMA covers the frequency range from 10.34 to 22.05 GHz having full width at half maximum (FWHM) of 11.71 GHz. The oblique incidents confirm that the peak absorption remains invariant up to 50° of incident angle. Moreover, the geometry is polarization insensitive in nature. The design mechanism is illustrated by the surface current distribution plot. The comparison of the proposed structure with the reference structures is explained in Table 1. From Table 1, it is observed that the proposed absorber structure has very compact size as compared to all other reference structures. Further, it provides the ultra-wideband absorption from 12 to 21 GHz and provides very good FWHM as compared to all other reference structures. Thus, it is confirmed that the proposed design is a very prominent structure in terms of size, UWB absorption, and FWHM.

Configuration and design of UWB absorber

The proposed UWB MMA is composed of three layers. The top layer consists of a resonating design and the bottom layer consists of a ground plane which is completely formed of metal. The metallic layer uses copper of thickness of 0.035 mm and

conductivity $\sigma = 5.96 \times 10^7$ S/m. The top and bottom layers are separated by a dielectric substrate FR-4 of thickness 1.54 mm and dielectric constant $\epsilon_r = 4.4$. The full-wave simulations and optimizations of the proposed absorber structure are accomplished with the use of finite integration technique (FIT)-based computer simulation microwave studio (CST MWS) [20] with periodic periphery conditions. However, the absorption rate $[A(\omega)]$ of the proposed absorber is calculated by equation $A(\omega) = 1 - |S_{11}(\omega)|^2 - |S_{21}(\omega)|^2$ where $S_{21}(\omega)$ is the transmission coefficient and $S_{11}(\omega)$ is the reflection coefficient. Since the ground surface is completely covered with metal, this prevents the incident wave transmission from one port to another port. Therefore, the transmission coefficient will be zero $[S_{21}(\omega) = 0]$ [21]. Thus, absorptivity can be calculated by $A(\omega) = 1 - |S_{11}(\omega)|^2$.

To interpret the wideband absorption mechanism, the design evolution of the proposed structure (design steps) and the corresponding absorption curve is shown in Figs 1(a) and 1(b), respectively. It is interestingly noticed that only single strip either vertical strip (Step-1) or horizontal strip (Step-2) provides very low absorption as clearly depicted in Fig. 1(b). However, individual diagonal strip (Step-3) resonates at 21 GHz with peak absorption of 80%. The absorption peak in Step-3 (diagonal strip) is higher than Step-1 (vertical strip) and Step-2 (horizontal strip) because eigenvalues vanishing identically corresponding to the number of holes result in resonances that are twofold degenerate

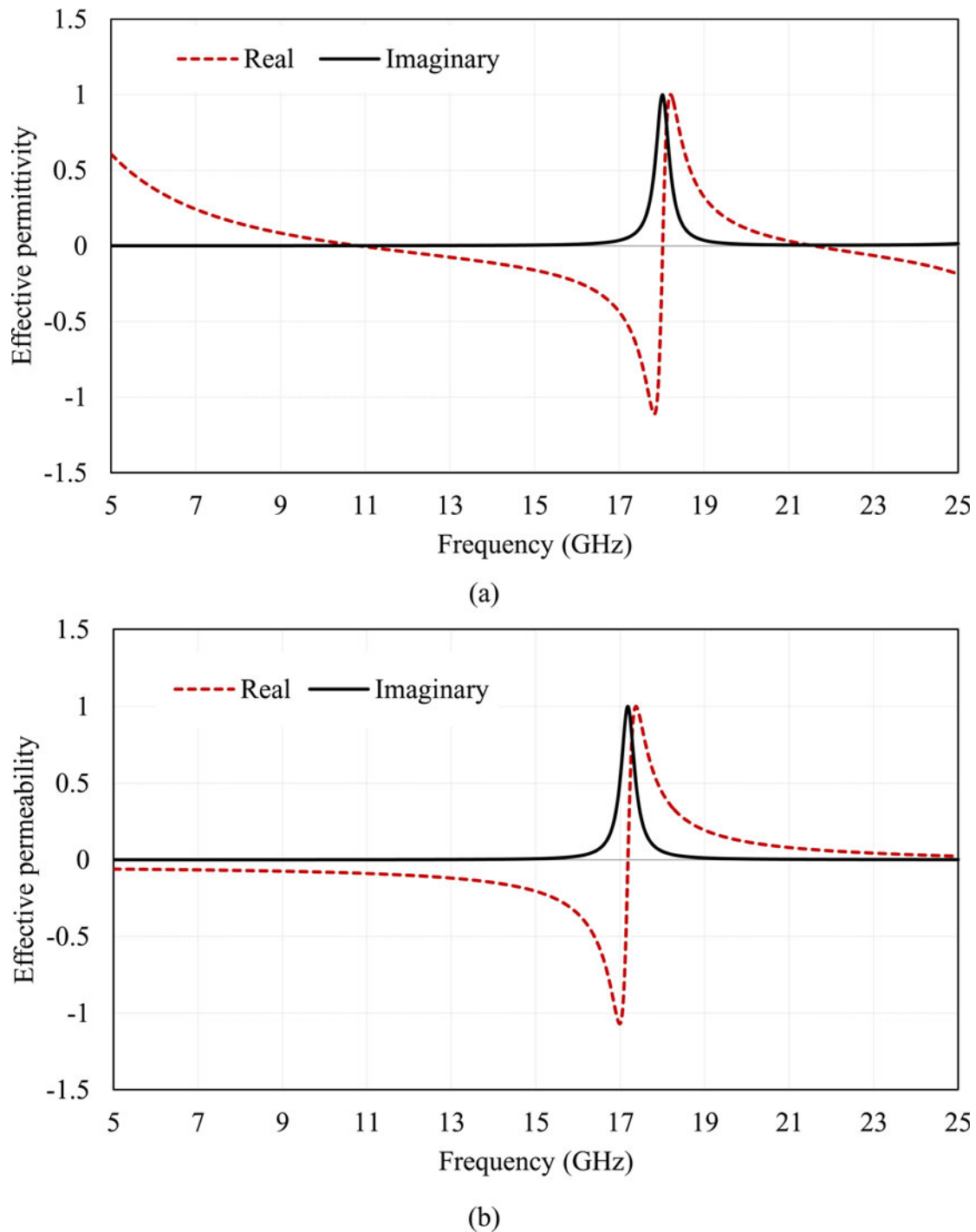


Fig. 4. (a) Effective permittivity of the proposed UWB absorber, (b) effective permeability of the proposed UWB absorber.

[22]. Further, the diagonal strip is added to the Step-1 and Step-2 resulting in Step-4 and Step-5 which are observed in the evolution process. The absorption peak for Step-4 and Step-5 is shown in Fig. 1(b). It is noticed that the combination of vertical strip and diagonal strip (Step-4) resonates at 18 GHz. However, the combination of horizontal strip and diagonal strip (Step-5) resonates at 16 GHz with very low absorption rate. Moreover, when we combine vertical strip and horizontal strip (Step-6), the absorption curve drastically changes, and provides a wideband absorption with a resonance peak at 14 and 18 GHz. Finally, to make

UWB nature of the proposed absorber, all three strips are combined together which not only introduces a strong coupling between them but also increases their corresponding capacitances. Hence, the proposed structure resonates at lower frequency i.e. 12 GHz along with the high absorption peaks at 17 and 21 GHz, as shown in Fig. 1(b). The strong mutual coupling among strips provides overlapping of the close resonances resulting in UWB absorption from 12 to 21 GHz with more than 97% absorptivity. Furthermore, interpretation of the resonances can also be explained by the surface current distribution as shown

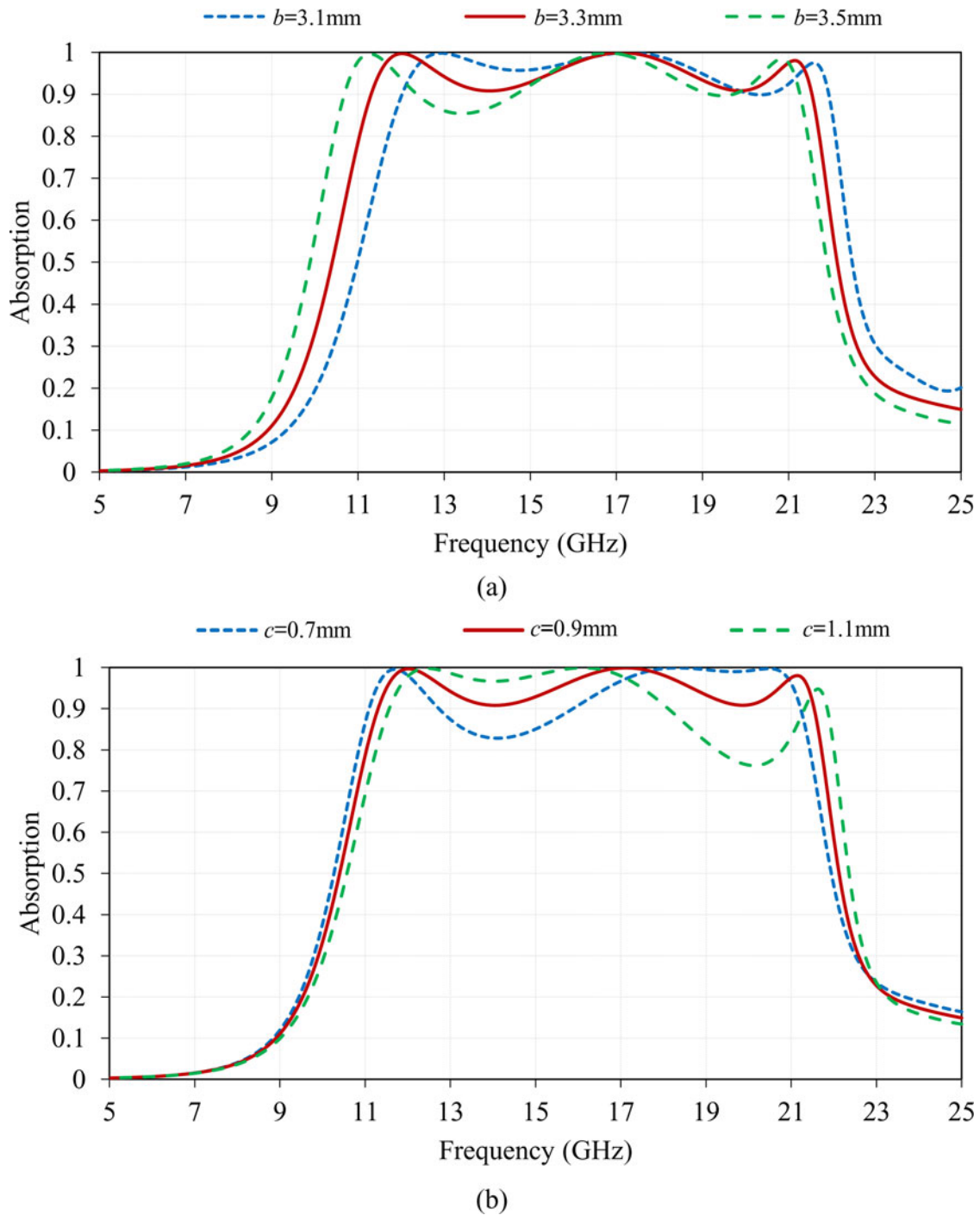


Fig. 5. (a) Effect of length of L-shaped structure “b”, (b) effect of width of L-shaped structure “c”.

in Fig. 2. It is noticed that at 12 GHz (lowest resonance), the almost same current density appears on vertical, horizontal, and diagonal strip due to which strong mutual coupling takes place. Therefore, the electrical length is increased and absorber resonates at 12 GHz with the peak absorption rate of 99%. However, maximum current is concentrated on inverted L-shaped strip at 17 GHz while equal current is concentrated at inverted L-shaped strip and diagonal strip at 21 GHz. From Fig. 1(b), it is interesting to notice that at 21 GHz, the resonance of diagonal

strip (Step-3) and inverted L-shaped strip (Step-6) cross each other, hence the same magnitude of the surface current appears at these strips.

Further, the normalized input impedance (Z_{in}) of the proposed UWB absorber, shown in Fig. 3 is calculated by using equation (1) [23]:

$$Z_{in} = \sqrt{\frac{(1 + S_{11})^2 - (S_{21})^2}{(1 - S_{11})^2 - (S_{21})^2}} \tag{1}$$

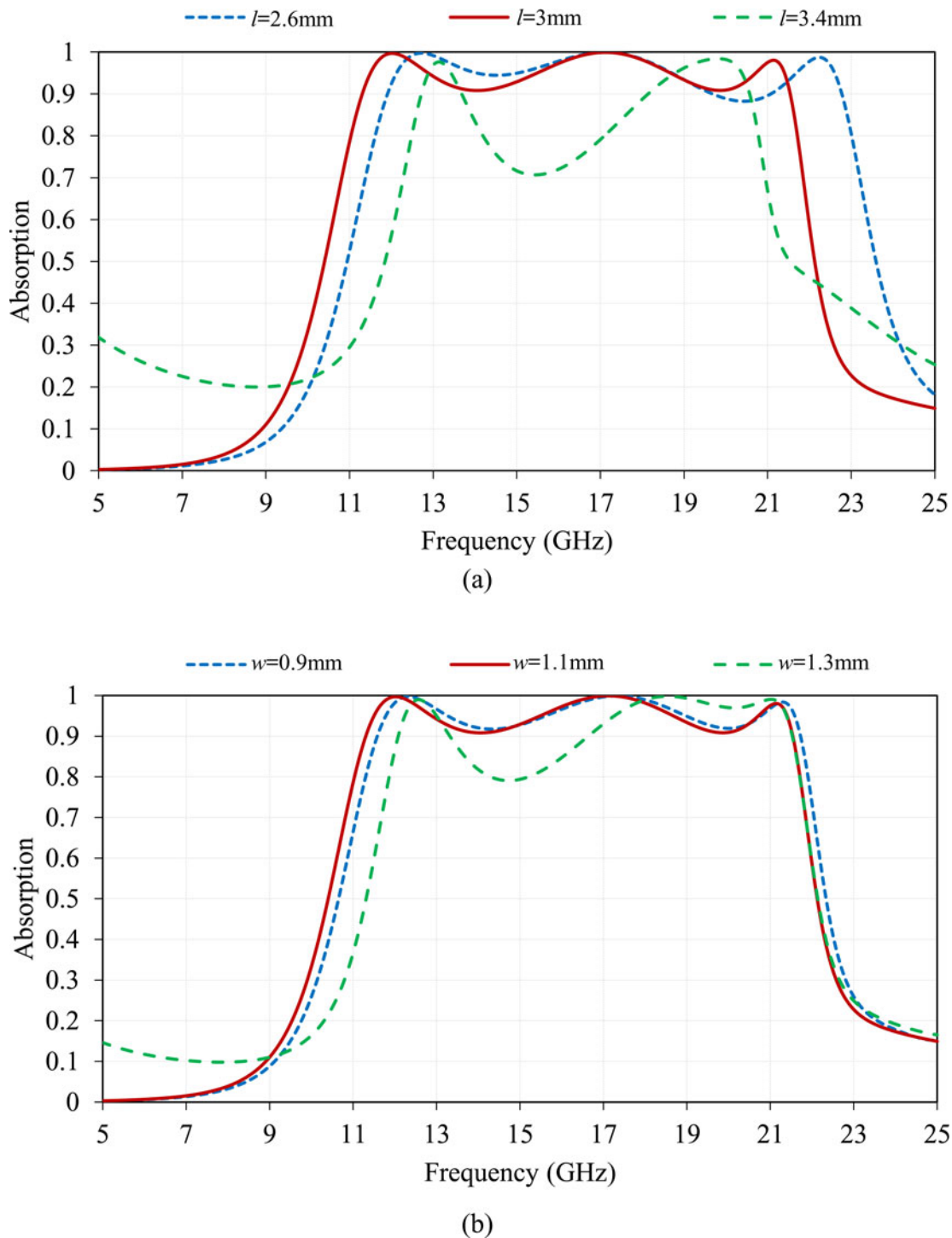


Fig. 6. (a) Effect of length of diagonally placed rectangular-shaped structure “ l ”, (b) effect of width of diagonally placed rectangular-shaped structure “ w ”.

It is observed that the imaginary part and the real part of the normalized input impedance becomes approximately equal to zero and unity, respectively, at the absorption peaks i.e. 12, 17, and 21 GHz. The unity value of the real part indicates the perfect impedance matching of the structure which leads to the maximum absorption.

Furthermore, the metamaterial characteristics i.e. effective permittivity (ϵ_{eff}) and effective permeability (μ_{eff}) of the proposed UWB absorber are analyzed and calculated using equation (2)

and (3), respectively:

$$\epsilon_{eff} = 1 + \frac{(2*j)(1 - S_{11} - S_{21})}{(k_0*d)(1 + S_{11} + S_{21})}, \quad (2)$$

$$\mu_{eff} = 1 + \frac{(2*j)(1 + S_{11} - S_{21})}{(k_0*d)(1 - S_{11} + S_{21})}, \quad (3)$$

where k_0 is the wavenumber of the free space and d is the thickness of a single unit cell of the structure. The obtained real and

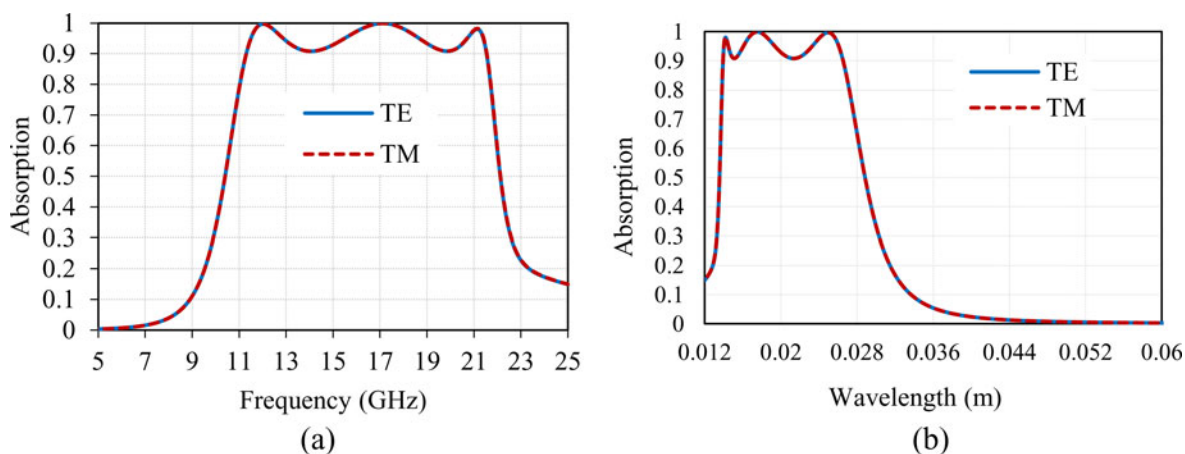


Fig. 7. (a) Absorption rate under TE and TM modes as a function of frequency, (b) absorption rate under TE and TM modes as a function of wavelength.

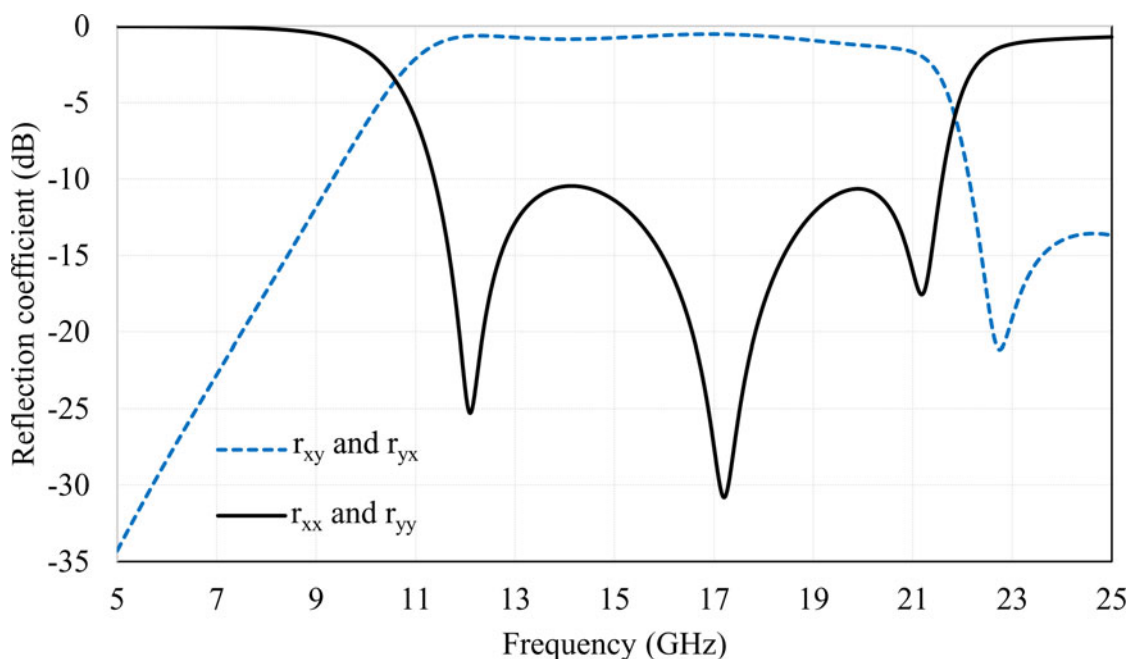


Fig. 8. Reflection coefficients of cross-polarization (r_{xy} and r_{yx}) and co-polarization (r_{xx} and r_{yy}).

imaginary parts of the effective permittivity (ϵ_{eff}) and effective permeability (μ_{eff}) are shown in Figs 4(a) and 4(b), respectively. The negative values of (ϵ_{eff}) and (μ_{eff}) in some part of the characteristic confirms that the proposed structure meets the metamaterial properties.

Parametric sensitivity

Further, the parametric sensitivity of the proposed absorber is observed by varying different parameters. Initially, the length “ b ” and width “ c ” of the L-shaped structure are varied keeping all other parameters fixed. It is observed from Fig. 5(a) that the increase in the length of the structure led to an increase in the inductance of the structure as a result of which the absorption

peak shifts towards the lower frequency side. Moreover, while increasing the width of the L-shaped geometry, the absorption peak shifts towards the higher frequency side due to the decrease in the corresponding capacitance of the geometry as shown in Fig. 5(b).

Furthermore, the effect of variation of parameters of the diagonally placed-rectangular shaped structure is also observed. It is observed from Figs 6(a) and 6(b) that while increasing the length “ l ” and width “ w ” of the diagonally placed-rectangular shaped structure, the bandwidth of the proposed wideband absorber decreases along with the decrease in the impedance matching and while decreasing the length of the diagonally placed-rectangular shaped structure, the absorption curve becomes wider but does not provide a good impedance matching.

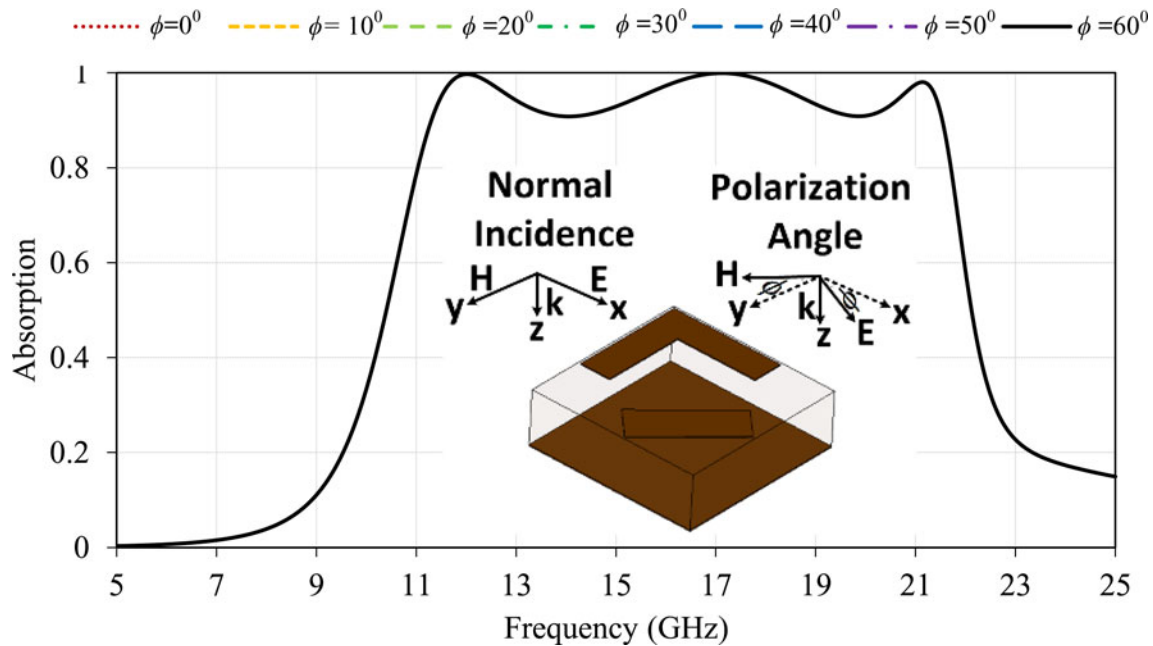


Fig. 9. Absorption response of proposed absorber with the variation of polarization angle (ϕ).

Analysis of simulated results

All the design, simulation, and optimization of the proposed absorber are carried out using CST MWS. The proposed UWB absorber structure is observed under the transverse electric (TE) mode as well as the transverse magnetic (TM) mode as a function of frequency and wavelength. It is observed that the proposed design provides the same bandwidth along with the same peak absorptivity for both (TE and TM) modes as presented in Fig. 7. Moreover, the structure resonates at frequency 7, 12, 17, 21 GHz and their corresponding wavelength i.e. 0.025, 0.017, and 0.014 m as shown in Figs 7(a) and 7(b), respectively. Further, in order to verify the property of MMA, the cross-polarization and co-polarization reflection coefficients are considered and shown in Fig. 8. The cross-polarization reflection coefficients (r_{xy} and r_{yx}) and the co-polarization reflection coefficients (r_{xx} and r_{yy}) are equal along x or y direction. Thus, we can consider only one polarization state for the incident wave [24]. It is observed from the figure that the cross-polarization reflection coefficient is approximately zero in the entire UWB band i.e. from 12 to 21 GHz whereas the co-polarization reflection coefficient is less than -10 dB and provides three dips near to 12, 17, and 21 GHz.

Furthermore, the proposed absorber is studied for the polarization sensitivity under the normal incidence angle. The direction of the wave vector is kept constant while the electric field and magnetic field directions are changed to examine the polarization behavior of the proposed structure. Although, no change is noticed under different polarization angles. It is clearly observed that as the polarization angle varies, the curves overlap each other thus making it polarization-insensitive in nature as shown in Fig. 9. Furthermore, the incident angle variation is analyzed to interpret its effect on the absorption rate as shown in Fig. 10. Firstly, the direction of the electric field is kept constant while the magnetic field and wave vector directions are varied by an angle θ as depicted in Fig. 10(a). Thereafter, the direction

of the magnetic field is kept constant while the electric field and wave vector directions are varied by an angle θ as depicted in Fig. 10(b). It is noticed that the absorption rate remains almost the same up to 50° as the incident angle varies from normal incidence to oblique incidence. However, beyond 50° of oblique incidence, absorption decreases and additional peaks appear close to higher resonance due to the theory of multiple reflection and interference [25].

Experimental validation

In order to impersonate the infinite periodicity of the unit cell, a 40×40 array of dimensions $200 \times 200 \text{ mm}^2$ of the proposed absorber is fabricated. The measurement setup contains a horn antenna, absorber holder, coaxial cables, and a network analyzer. The measurement is carried out using Keysight ENA series network analyzer E5063A (100 KHz -18 GHz) however, the plot is showing upto 25 GHz. The measured result of the proposed absorber is closely matched upto 18 GHz (the maximum range of network analyzer). Moreover, the measured result beyond 18 GHz is predicted based on the simulated data and measured data (upto 18 GHz).

The measurement setup of the fabricated prototype of the proposed absorber is shown in Fig. 11(a). The fabricated proposed absorber structure is positioned in forefront of the horn antenna at a distance 60 cm (far-field). Initially, the reflectance of the backplane (completely metallic) of the absorber is measured thereafter, the reflectance of the front side of MMA is measured. Then, metamaterial reflectance is normalized by backplane (metallic plate) reflectance. Finally, measured absorption is obtained which is compared with the simulated one as shown in Fig. 11(b). The minor variations between simulated and measured results are noticed. The fabrication tolerances and free space measurement inaccuracies have often led to these minor variations in the measured and simulated results.

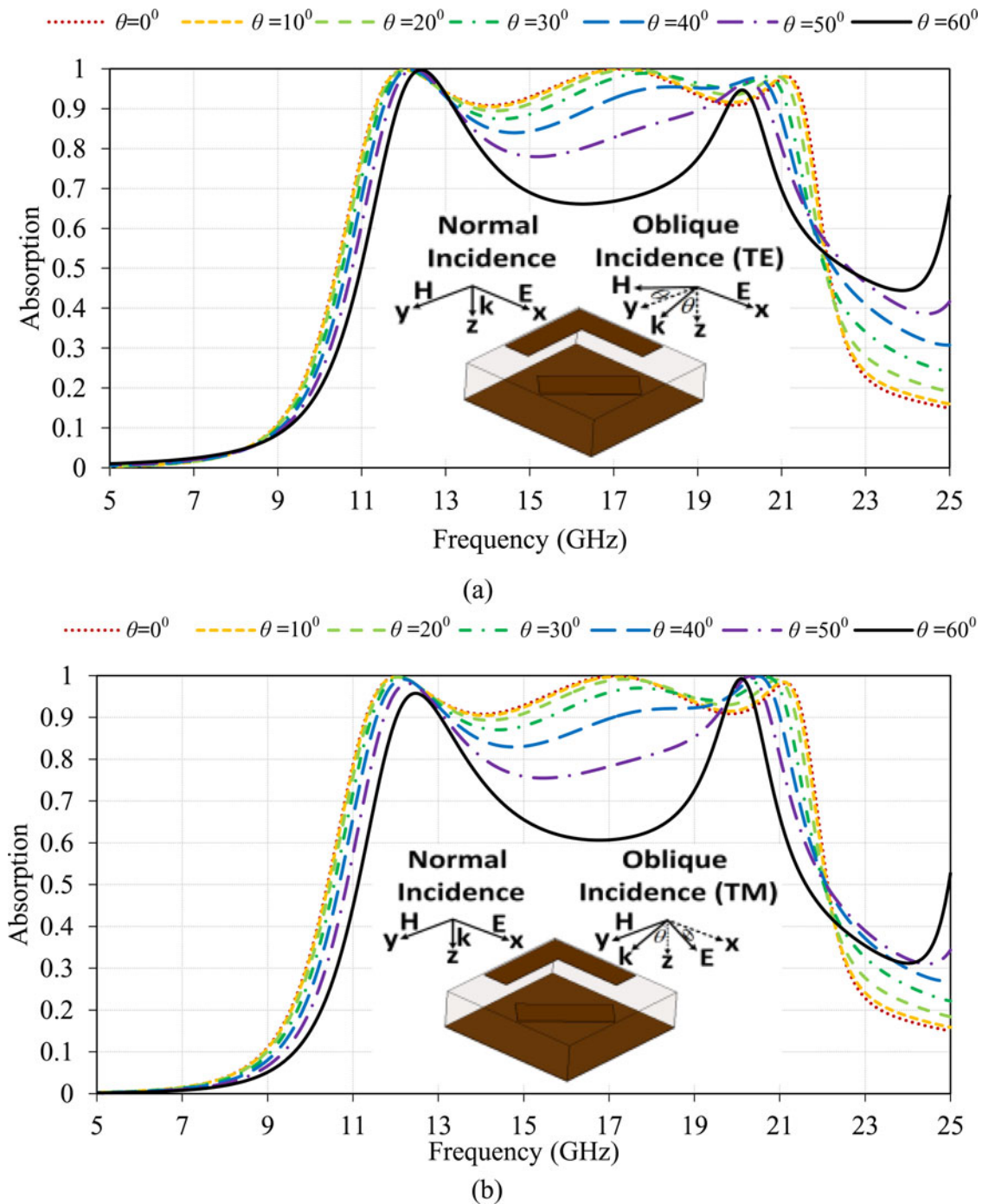


Fig. 10. (a) Absorption response of proposed absorber with the variation of incident angle (θ) for TE polarized wave, (b) absorption response of proposed absorber with the variation of incident angle (θ) for TM polarized wave.

Conclusion

In this paper, a super-compact UWB MMA has been analyzed. The unit cell configurations of the proposed structure are optimized to get the wider bandwidth with high absorption. The measured results confirm the proposed MMA achieving UWB absorptivity from 12 to 21 GHz with FWHM of 11.71 GHz. The absorption rate is more than 97% over the entire range of frequency. Further, the parametric sensitivity of the proposed absorber is observed by varying different parameters. Moreover,

the polarization sensitivity and the consequence of incident angle are analyzed and observed the insignificant change is observed in peak absorption with the variation of polarization angle (ϕ) and small variation in peak absorption with the variation of incidence angle (θ). The proposed MMA is compared with reference absorber and observed that it is super compact with respect to size and has a wide bandwidth and FWHM. The proposed MMA covers Ku and K bands approximately and, therefore, has different quality applications in stealth

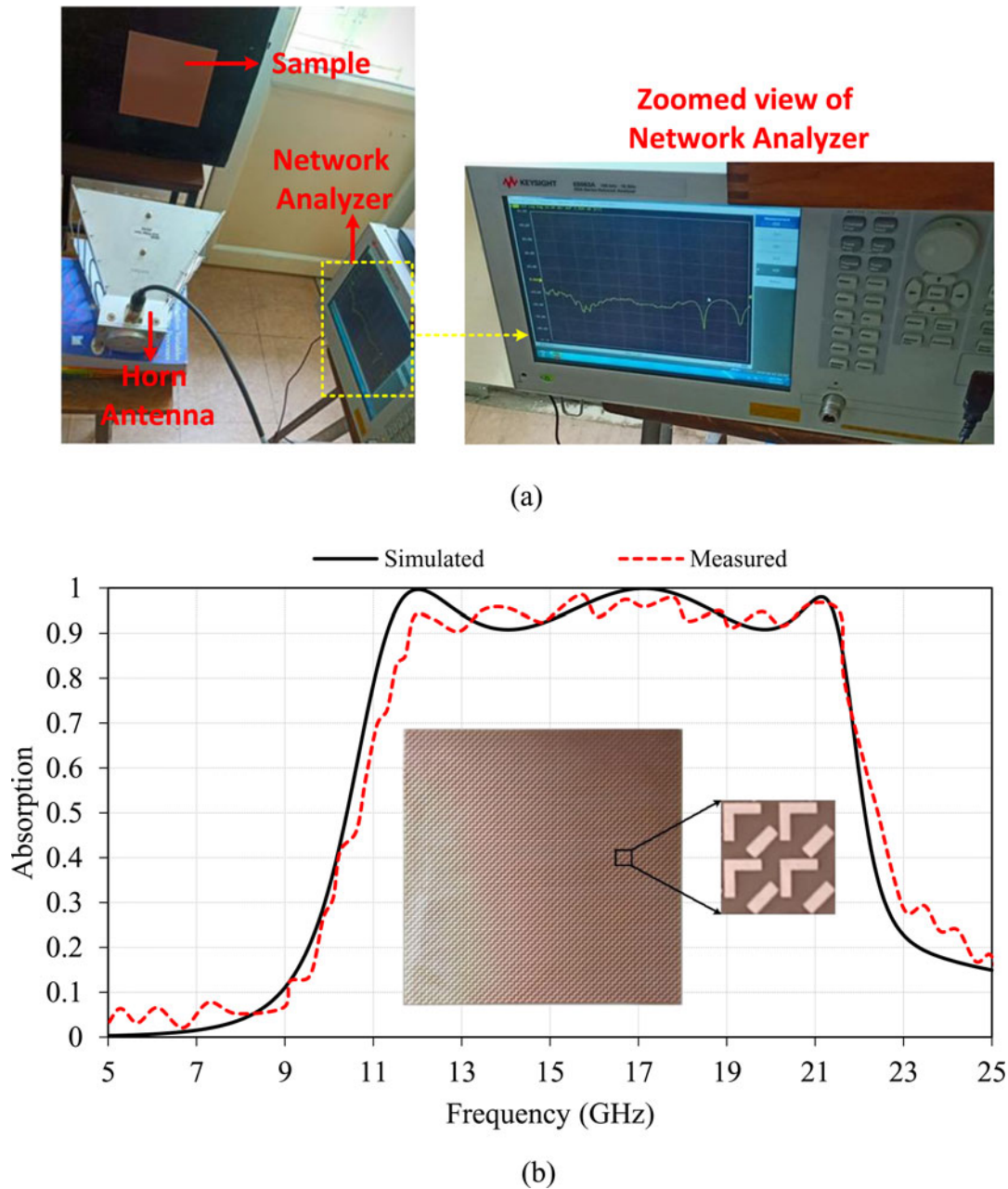


Fig. 11. (a) The measurement setup of the fabricated prototype of the proposed absorber, (b) the comparison of the simulated and the measured results.

technology, thermal imaging, detection, antenna systems, and other EM devices.

Acknowledgements. The authors would like to thank Department of Electronics and Communication Engineering, TIET, Patiala, Punjab for providing necessary instrument facility to carry out the measurement and would also like to thank Thapar Institute of Engineering and Technology, Patiala, Punjab for providing seed money grant as financial support to carry out this research.

References

1. Smith DR, Padilla WJ and Vier DC (2000) Composite medium with simultaneously negative permeability and permittivity. *Physical Review Letters* **84**, 4184–4187.
2. Fang N, Lee H, Sun C and Zhang X (2005) Sub-diffraction-limited optical imaging with a silver superlens. *Science (New York, N.Y.)* **308**, 534–537.
3. Schurig D, Mock JJ, Justice BJ, Cummer SA, Pendry JB, Starr AF and Smith DR (2006) Metamaterial electromagnetic cloak at microwave frequencies. *Science (New York, N.Y.)* **314**, 977–980.
4. Landy NI, Sajuyigbe S and Mock JJ (2008) Perfect metamaterial absorber. *Physical Review Letters* **100**, 207402, (1–4).
5. Erentok A and Ziolkowski RW (2008) Metamaterial-inspired efficient electrically small antennas. *IEEE Transactions on Antennas and Propagation* **56**, 691–707.
6. Chaimool S, Chung KL and Akkaraekthalin P (2009) A 2.45-GHz WLAN high-gain antenna using a metamaterial reflecting surface. *The International Symposium on Antennas and Propagation (ISAP)*, October 20–23, Bangkok, Thailand, pp. 325–328.
7. Chung KL and Kharkovsky S (2013) Metasurface-loaded circularly-polarised slot antenna with high front-to-back ratio. *Electronics Letters* **49**, 979–981.

8. **Jiang J, Xia Y and Li Y** (2019) High isolated X-band MIMO array using novel wheel-like metamaterial decoupling structure. *ACES Journal* **34**, 1829–1836.
9. **Bhattacharyya S, Ghosh S, Chaurasiya D and Srivastava KV** (2014) A broadband wide angle metamaterial absorber for defense applications. *IEEE International Microwave and RF Conference (IMaRC)*, 33–36.
10. **Wang BY, Liu SB, Bian BR, Mao ZW, Liu XC, Ma B and Chen L** (2014) A novel ultrathin and broadband microwave metamaterial absorber. *Journal of Applied Physics* **116**, 094504, (1–7).
11. **Li S, Guo J, Cao X, Li W, Zhang Z and Zhang D** (2014) Wideband, thin, and polarization-insensitive perfect absorber based on the double octagonal rings metamaterials and lumped resistances. *Journal of Applied Physics* **116**, 043710.
12. **Yuan W and Cheng Y** (2014) Low-frequency and broadband metamaterial absorber based on lumped elements: design, characterization and experiment. *Applied Physics A, Materials Science & Processing* **117**, 1915–1921.
13. **Sood D and Tripathi CC** (2015) A wideband wide-angle ultra-thin metamaterial microwave absorber. *Progress in Electromagnetics Research M* **44**, 39–46.
14. **Sekar R and Inabathini SR** (2018) An ultra-thin compact wideband metamaterial absorber. *Radio Engineering* **27**, 364–372.
15. **Barde C, Choubey A and Sinha R** (2019) A set square design metamaterial absorber for X-band applications. *Journal of Electromagnetic Waves and Applications* **34**, 1430–1443.
16. **Ranjan P, Choubey A, Mahto SK, Sinha R and Barde C** (2019) A novel ultrathin wideband metamaterial absorber for X-band applications. *Journal of Electromagnetic Waves and Applications* **33**, 2341–2353.
17. **Wang Q and Cheng Y** (2020) Compact and low-frequency broadband microwave metamaterial absorber based on meander wire structure loaded resistors. *International Journal of Electronics and Communications (AEÜ)* **120**, 153198, (1–8).
18. **Wu X, Li Y and Liu X** (2019) High-order dual-port quasi-absorptive microstrip coupled-line bandpass filters. *IEEE Transactions on Microwave Theory and Techniques*, 1–14. Doi: 10.1109/TMTT.2019.2955692.
19. **Jeong SW, Lee TH and Lee J** (2019) Frequency- and bandwidth-tunable absorptive bandpass filter. *IEEE Transactions on Microwave Theory and Techniques* **67**, 2172–2180.
20. **CST Microwave Studio available**, <http://www.cst.com>.
21. **Mishra N, Kumari K and Chaudhary RK** (2018) An ultra-thin polarization independent quad-band microwave absorber-based on compact metamaterial structures for EMI/EMC applications. *International Journal of Microwave and Wireless Technologies* **10**, 422–429.
22. **Kruger F and Scheidl S** (2003) Spin dynamics of stripes. *Physical Review B* **67**, 134512, (1–11).
23. **Kalraiya S, Chaudhary RK, Abdalla MA and Gangwar RK** (2019) Polarization and incident angle independent metasurface absorber for X-band application. *Material Research Express* **6**, 045802, (1–8).
24. **Zhao J and Cheng Y** (2016) A high-efficiency and broadband reflective 90° linear polarization rotator based on anisotropic metamaterial. *Applied Physics B: Photophysics and Laser Chemistry* **255**, 1–7.
25. **Wanghuang T, Chen W, Huang Y and Wen G** (2013) Analysis of metamaterial absorber in normal and oblique incidence by using interference theory. *AIP Advances* **3**, 102118, (1–3).



Manpreet Kaur received her B.Tech. degree in Electronics and Communication Engineering from the Punjabi University, Patiala, India in 2017 and M.Tech. degree in Electronics and Communication Engineering from the Thapar Institute of Engineering and Technology, India. Currently, she is pursuing her Ph.D. degree in the Department of Electronics and Communication Engineering, Thapar Institute of Engineering and Technology, Patiala, India. Her research interests include MIMO antennas, metamaterial absorbers, electromagnetic band gap structures, and so on. She has published three papers in various peer-reviewed international journals and conferences.



Hari Shankar Singh was born in Sonbhadra (U.P.), India, in 1990. He received his B.Tech. degree from the IEC College of Engineering and Technology, Greater Noida (U.P.), India, in 2011 and Ph.D. degree from the Department of Electronics Engineering, Indian Institute of Technology, Banaras Hindu University, India, in 2015. Currently, he is working as Assistant Professor in the Department of Electronics and Communication Engineering, Thapar University, Patiala, Punjab. His research interests include microstrip antennas, MIMO antenna systems, ultrawideband (UWB) antennas, metamaterial absorbers, electromagnetic bandgap (EBG) structures, RFID antennas, mobile antennas, and multiple antenna–user interactions. His Ph.D. thesis has been awarded the best under the category of Ph.D. symposium in IEEE UPCON 2016, held at IIT (BHU), Varanasi. He has published more than 70 papers in various peer-reviewed international journals and conferences.